# Asymmetric alkoxy and alkyl substitution on non-fullerene acceptors enabling high-performance organic solar cells

Yuzhong Chen, Fujin Bai, Zhengxing Peng, Lei Zhu, Jianquan Zhang, Xinhui Zou, Yunpeng Qin, Ha Kyung Kim, Jun Yuan, Lik-Kuen Ma, Jie Zhang, Han Yu, Philip C.Y. Chow, Fei Huang, Yingping Zou, Harald Ade, Feng Liu*, He Yan*

Dr. Y. Chen, F. Bai, Dr. J. Zhang, X. Zou, H. Kim, Dr. L.-K. Ma, H. Yu, Dr. P. Chow, Prof. H.Yan

Hong Kong University of Science and Technology-Shenzhen Research Institute, No. 9 Yuexing first RD, Hi-tech Park, Nanshan, Shenzhen 518057, P. R. China

Email: hyan@ust.hk

Dr. L. Zhu, Prof. F. Liu

School of Physics and Astronomy, and Collaborative Innovation Center of IFSA (CICIFSA), Shanghai Jiao Tong University, Shanghai 200240, P. R. China

Email: fengliu82@sjtu.edu.cn

Dr. Z. Peng, Dr. Y. Qin, Prof. H. Ade

Department of Physics and Organic and Carbon Electronics Laboratories (ORaCEL), North Carolina State University, Raleigh, NC 27695, USA

This is the author manuscript accepted for publication and has undergone full peer review but has not been through the copyediting, typesetting, pagination and proofreading process, which may lead to differences between this version and the Version of Record. Please cite this article as doi: 10.1002/aenm.202003141.

Dr. Y. Chen, F. Bai, Dr. J. Zhang, X. Zou, H. Kim, Dr. L.-K. Ma, H. Yu, Dr. P. Chow, Prof. H.Yan

Department of Chemistry, Energy Institute and Hong Kong Branch of Chinese National Engineering Research Center for Tissue Restoration & Reconstruction, Hong Kong University of Science and Technology, Clear Water Bay, Kowloon, Hong Kong

Dr. J. Yuan, Prof. Y. Zou

College of Chemistry and Chemical Engineering, Central South University, Changsha 410083, P. R. China

Dr. Jie Zhang, Prof. F. Huang, Prof H. Yan,

Institute of Polymer Optoelectronic Materials and Devices, State Key Laboratory of Luminescent Materials and Devices, South China University of Technology (SCUT), Guangzhou 510640, P. R. China

Y. Chen and F. Bai contributed equally to this work.

## Abstract

In this paper, we report a strategy of asymmetric alkyl and alkoxy substitution that is applied to state-of-the-art Y-series non-fullerene acceptors (NFAs) and achieve great performance in organic solar cell (OSC) devices. As alkoxy groups can have significant influence on the material properties of NFAs, we first apply alkoxy substitution on the Y6 molecule in a symmetric manner. The resulting molecule (named Y6-2O), despite showing improved open-circuit voltage ($V_{oc}$), yielded extremely poor performance due to low solubility and excessive aggregation property, a change owing to the conformational locking effect of alkoxy groups. Our novel strategy is to apply asymmetric alkyl and alkoxy substitution on Y6, yielding a molecule named Y6-1O that can maintain the positive effect of $V_{oc}$ improvement and obtain reasonably good solubility. The resulting molecule Y6-1O enables highly efficient non-fullerene OSCs with 17.6% efficiency and our asymmetric side-chain strategy has the potential to be applied to other NFA-material systems to further improve their performances.

**Keywords**: Organic solar cells, Y-series acceptors, Asymmetric alkoxy substitution, Solubility, Morphology

## Introduction

During the past several years, the emergence of high-performance non-fullerene acceptors (NFAs) has revolutionized the field of organic solar cells (OSCs), as NFAs can offer easily tunable chemical structures and energy levels leading to high efficiencies and great stability.[1-8] Currently, power conversion efficiencies (PCEs) over 16% have been reached by several state-of-the-art NFAs-based systems,[9-19] most of which are based on Y-series NFAs.[20-22] The devices based on a typical Y-series NFA (Y6) can achieve a small voltage loss (0.5 V) while maintaining excellent short-circuit current density ($J_{sc}$) and fill factor (FF). This new family of NFA materials has the potential to push OSC efficiencies toward 20%.

Rational molecular design of NFAs then becomes a critically important area of research. Due to its excellent performance, Y6 has become an important topic of study recently and it is important to understand its structure-property relationship and the key structural features of Y6 that may contribute to its good performance. Some papers show that the branched alkyl chains on the pyrrole motif can have a great impact on the solubility of the molecule and the morphology of the blend films, resulting in different performances in final devices.[23-25] Another important structural feature is the straight alkyl chains on the β-position of the outer thiophene unit, which is not studied in detail yet.

One of the widely used strategies to modify alkyl chains is to replace them with alkoxy side chains. The alkoxy chains can have a significant influence on the electronic and

morphological properties of organic semiconductor molecules.[26-33] First, they can change the electrical properties of the conjugated molecule due to the electron-donating effect of alkoxy groups.[34, 35] Besides, the oxygen atoms can have the effect of intramolecular conformational locking effect in some molecular structures, which could change the aggregation property of the molecule thus the morphology of the blends.[36-39] In previous reports, alkoxy substitution has been used on IEIC-type small molecules. [40-42] After alkoxy modification on IEIC, the resulting molecule IEIC-O shows a significant red-shifted spectrum to the near-infrared region, which is beneficial for high $J_{sc}$ but may reduce the open-circuit voltage ($V_{oc}$) of the corresponding devices. Therefore, it is interesting to consider the modification of Y6 molecules with alkoxy side chains.

In this work, we first attempt to modify Y6 with alkoxy chains in a symmetric manner and find that the resulting molecule (named Y6-2O) exhibits poor solubility (1.5 mg/mL in chloroform) and excessive aggregation property due to the conformational locking effect of alkoxy groups (despite showing some positive effects on $V_{oc}$ improvement). To address the negative influence of alkoxy chains, we adopt a novel asymmetric alkyl and alkoxy substitution strategy by attaching one alkoxy chain on one side of the molecule (on the β position of thienothiephene unit) and one alkyl chain on the other side.[43] The asymmetric molecule (named Y6-1O) can achieve a reasonably good solubility (20 mg/mL) and morphology while maintaining the beneficial electronic effect of the alkoxy groups. As a result of asymmetric alkoxy and alkyl substitution, we achieve a highly efficient binary (16.1%) and ternary (17.6%) OSCs when incorporating $PC_{71}BM$ as the third component. This

asymmetric side-chain substitution strategy can be potentially applied to other material systems to help tune the solubility and electronic properties of the NFAs and thus achieving better performances.

## Result and discussion

The chemical structures of Y6-2O, Y6-1O and Y6 are shown in **Figure 1a**. The main difference between Y6, Y6-1O and Y6-2O is the number of substitution of the undecyloxy group on the β-position of the outer thiophene unit. Compared to Y6, Y6-1O has one undecyloxy substitution on one side of the outer thiophene unit, while Y6-2O has one undecyloxy substitution on each side. The synthesis routes of Y6-1O and Y6-2O shown in **Schemes S1** and **Schemes S2** are similar to that of Y6.[20] Corresponding nuclear magnetic resonance spectra and mass spectra of the intermediate compounds and final small molecules are displayed in **Supporting Information**. Y6-1O can be well dissolved in common organic solvents such as dichloromethane and chloroform, but Y6-2O has very poor solubility even in chloroform. Using reported procedures, the solubility of Y6, Y6-1O and Y6-2O in chloroform is estimated to be 40 mg/mL, 20 mg/mL and 1.5 mg/mL, respectively.[23] This result shows that the asymmetric strategy can address the problem of poor solubility after symmetric alkoxy substitutions. According to thermogravimetric analysis results (TGA, **Figure S1a**), the decomposition temperature ($T_d$, 5% weight loss) of Y6, Y6-1O and Y6-2O are 323 $^{o}$C, 328 $^{o}$C and 333 $^{o}$C, which indicates their great thermal stability. Differential scanning calorimetry (DSC) was applied to further investigate the molecular aggregation and

crystallinity of three acceptors, as shown in **Figure S1b**. Upon heating, Y6 exhibits a melting peak at the temperature of 297 ℃ with an enthalpy change of 27.33 J $g^{-1}$ while the melting peak of Y6-1O is at higher temperature of 314 ℃ with an enthalpy change of 35.20 J $g^{-1}$, which implies that Y6-1O has better molecular packing and stronger crystallinity than Y6. However, Y6-2O did not show any melting peak before its decomposition temperature, which indicates its melting point should be higher than 330 ℃. Therefore, Y6-2O may have the strongest molecular packing and crystallinity that cause the poor solubility. The DSC measurement has clearly shown that the introduction of alkoxy side chains facilitate intermolecular packing of the resulting molecules.

**Figure S2a** shows the absorption spectra of the three molecules in chloroform solution. All three small molecules have strong absorption in the range of 600-750 nm, and that Y6-2O and Y6-1O exhibit relatively blue-shifted spectra in comparison to that of Y6. The maximum molar extinction coefficients of Y6-2O, Y6-1O and Y6 are $1.90\times10^5$, $2.00\times10^5$ and $1.87\times10^5$ $M^{-1}$ $cm^{-1}$ at 701, 715 and 732 nm, respectively (**Table 1**). Compared to the absorption in solution, obvious redshifts and vibration shoulder peaks arise in the absorption spectra of three neat films, which implies their strong π-π stacking in the solid state (**Figure 1b**). Similar to the absorption in solution, the substitution of the alkoxy groups causes more blue-shifted spectra from Y6, Y6-1O to Y6-2O in neat films. Therefore, the bandgaps of Y6, Y6-1O and Y6-2O calculated from the onset of film absorption increase gradually, which are 1.35 eV, 1.43 eV and 1.45 eV, respectively (**Table 1**). To further investigate the effect of alkoxy substitution on the bandgaps and energy levels, cyclic voltammetry (CV)

measurement is carried out by using $Ag/Ag^+$ as the reference and $Fc/Fc^+$ (-4.80 eV) as the standard. The corresponding CV plots are shown in **Figure S3**. It can be estimated from the plots that the HOMO levels of Y6, Y6-1O and Y6-2O are almost the same, but the LUMO levels upshift from -3.89 eV, -3.84 eV to -3.76 eV (**Figure 1c** and **Table 1**). Overall, the UV-vis spectra and CV results indicate that the alkoxy substitution can upshift the LUMO level without changing the HOMO level significantly, which could lead to a higher $V_{oc}$ of the corresponding OSCs.

To understand the influence of the alkoxy substitution on molecular geometries and energy level of the molecules, density functional theory (DFT) calculations were carried out at B3LYP/6-31G* level by simplifying the long side chains with methyl, ethyl or methoxy groups. As summarized in **Table S1**, the top-view and side-view geometry of Y6-2O, Y6-1O and Y6 are almost the same, indicating no significant changes of geometry caused by the alkoxy groups. Because of the second branched alkyl chain on the nitrogen, Y6-2O, Y6-1O and Y6 all have slightly twisted structure, which can keep the molecules from over-aggregation.[20] According to the calculation results, the HOMO levels of Y6, Y6-1O and Y6-2O are almost the same while the LUMO levels are increased from -3.54 eV, -3.49 eV to -3.38 eV. These calculation results are consistent with the CV measurements and UV-vis spectra, which further supports the effects of alkoxy substitution as mentioned earlier.

To understand the reason for the dramatically reduced solubility (from Y6 to Y6-2O) caused by alkoxy substitution, we further carried out DFT calculations to investigate the

conformational locking effect of the alkoxy groups on these molecules.[44-46] To simplify the calculations, we focus on the structure area with possible intramolecular conformational locking and compare two simplified units named T-O-IC and T-C-IC which are parts of Y6-2O and Y6 (**Figure 2a**). We set the optimized structure of T-O-IC and T-C-IC as the starting point. Then relaxed potential energy scans (PES) were taken by DFT calculation at B3LYP/6-31G* level, in which the torsion axis is the single bond between the thiophene unit and the end groups (**Figure 2a**). As PES results shown in **Figure 2b**, since the torsion barrier between A and B or A and F in T-O-IC is higher than that in T-C-IC unit (around 15 kJ/mol difference), conformation A is more preferred in T-O-IC than T-C-IC. The PES results indicate that the alkoxy side chains have a stronger conformational locking effect than alkyl side chains, which could increase the aggregation property of the molecule and also reduce its solubility. Besides, the energy-preferred conformation of A shown in **Figure 2c** suggests that the methyl group attached to the oxygen atom in T-O-IC prefers to stay in the plane of conjugated backbone while that attached to the carbon atom in T-C-IC tends to be slightly out of the plane, which is also found in the side-view geometry of Y6, Y6-1O and Y6-2O (**Table S1**). This small difference could also facilitate the molecular packing of alkoxy-substituted molecules and decrease their solubility. In addition, the dipole moment of Y6, Y6-1O and Y6-2O (in their optimized structure) are also calculated and the results are listed in **Table S1**. The enhanced dipole moment from Y6 (1.037 D), Y6-1O (1.953 D) to Y6-2O (3.656 D) indicates that alkoxy substitution can bring stronger intermolecular interactions.[47, 48]

A large-bandgap polymer PM6 (**Figure 1d**) was chosen as the polymer donor due to its proper absorption (**Figure 1b**) and matching energy level with these three acceptors (**Figure 1c**).[49-51] The devices were made with the structure of ITO/ PEDOT: PSS /PM6: NFA/ PNDIT-F3N /Ag, in which the PM6: NFA weight ratio is controlled at 1: 1.2 with the concentration of PM6 at 8 mg/mL. Chloroform is chosen as the processing solvent, and 1-chloronaphthalene (CN) is chosen as the additive (0.5%, v/v). Because of the poor solubility of Y6-2O in chloroform, hot solvent is used to dissolve PM6 and Y6-2O first and then a quick spin-coat process is performed to make the active layers. The thickness of the active layers is kept at about 100 nm, and the annealed temperature is set at 100 $^{o}$C to achieve better morphology. The optimal photovoltaic parameters of Y6-2O, Y6-1O and Y6 based OSCs are summarized in **Table 2** with corresponding *J*-*V* curves in **Figure 3a**. The $V_{oc}$ is increased from Y6 (0.82 V), Y6-1O (0.89 V) to Y6-2O (0.92 V), which agrees with energy level alignment in **Figure 1c**. The PM6: Y6-2O based devices exhibited quite low $J_{sc}$ and FF, which results in an inferior efficiency of 6.6%. Compared to OSCs based on PM6: Y6, although OSCs based on PM6: Y6-1O show a slightly lower $J_{sc}$ of 23.2 mA cm$^{-2}$, they can achieve an enhancement in $V_{oc}$ of 0.89 V and high FF of 78.3%. Therefore, a high PCE of 16.1% can be achieved by Y6-1O based devices, which is one of the highest values in binary systems. **Table S2** summarizes the mean values and standard deviations of photovoltaic parameters collected from 20 devices of each acceptor, which proves their good reproducibility. According to the device results, the asymmetric alkoxy and alkyl substitution can help improve $V_{oc}$ significantly while keeping high FF to achieve better PCEs.

In order to investigate the reason for the difference of $J_{sc}$ among the Y6-2O, Y6-1O and Y6 based devices, EQE measurements were acquired and the corresponding spectra are shown in **Figure 3b**. The $J_{sc}$ of Y6-2O, Y6-1O and Y6 based devices calculated from the EQE spectra are reasonably agreed with the $J_{sc}$ obtained from the *J-V* curves (**Table 2**). For PM6: Y6-1O and PM6: Y6 based devices, the EQE spectra are consistent with corresponding blend films absorption (**Figure S2b**), and EQE can reach above 70% in their absorption range. For PM6: Y6-2O based devices, however, the EQE can only maintain around 40% in their absorption range. According to the EQE data, the integrated $J_{sc}$ of PM6: Y6-1O and PM6: Y6 based devices in the wavelength range of 800 - 1000 nm were calculated, which are 2.73 mA $cm^{-2}$ and 4.35 mA $cm^{-2}$, respectively. The integrated $J_{sc}$ difference of 1.62 mA $cm^{-2}$ in the range of 800 - 1000 nm accounts for majority of the total integrated $J_{sc}$ difference (1.9 mA $cm^{-2}$). The EQE results reveal that the decreased $J_{sc}$ from Y6 based devices to Y6-1O based devices is mainly caused by the blue-shifted absorption onset.

Photoluminescence (PL) intensity of the Y6, Y6-1O and Y6-2O based films was measured to understand the difference in their EQE spectra. The corresponding PL spectra excited at 785 nm are shown in **Figure 3c-e**. The PL quenching efficiency of PM6: Y6-2O blends is just 30.2%, which indicates that less free charges can be generated in the blends and results in a low EQE of the Y6-2O-based devices. The PL quenching efficiency of PM6: Y6-1O blends is 95.7% while the PL quenching efficiency of PM6: Y6 blends is 95.2%, which explains the similar and high EQE of the corresponding devices.

To better understand the effects of the alkoxy substitution on morphology, 2D grazing incidence wide-angle X-ray scattering (GIWAXS) measurements were performed on pure and blend films.[52] The GIWAXS patterns and corresponding 10° sector averaged GIWAXS profiles are shown in **Figure 4** with the analysis results of (010) peak shown in **Table 3**. For the pure film, there is no distinct difference between Y6-1O and Y6. Nevertheless, Y6-2O has extremely high aggregation property, which can be proved by the appearance of the higher-ordered lamellar peak (200) in the 2D patterns and extremely high coherence length of (010) π-π stacking (**Table 3**). PM6: Y6-1O and PM6: Y6 blends both exhibit strong (010) peaks in the out-of-plane direction and the (100) in the in-plane direction, which implies they both take face-on orientations. PM6: Y6-2O blend shows the (010) and (100) in both in out-of-plane and in-plane direction, suggesting the mixed face-on and edge-on orientation, which is not beneficial for the charge transportation.[53]

Furthermore, the (010) d-spacing and coherence length for PM6: Y6-1O are 3.51 Å and 29 Å, which is similar to that of the PM6: Y6 blend. For the PM6: Y6-2O blend, however, it exhibits extremely poor film quality even by naked eyes due to the poor solubility of Y6-2O. Note that the 2D-GIWAXS patterns of PM6: Y6-2O is quite similar with that of pure PM6, which indicates that PM6 and Y6-2O cannot mix well due to the poor solubility of Y6-2O so that most area of the film is only made by PM6. But still, there are a lot of diffraction signals in the PM6: Y6-2O pattern, supporting the higher aggregation property of Y6-2O than Y6-1O or Y6. The GIWAXS results indicate that alkoxy groups can increase molecular packing (presumably due to the intramolecular conformational locking effect) and aggregation

property, which also explains the poor solubility of the Y6-2O molecule. For the Y6-1O molecule, however, the asymmetric nature of the molecule probably helps to minimize the problem of excessive molecular packing of Y6-2O. As a result, the Y6-1O molecule can achieve reasonably good solubility and aggregation property and thus great performance.

Next, resonant soft X-ray scattering (R-SoXS) was used to understand the nanoscale morphology of the three blends.[54] The corresponding profiles of R-SoXS results are shown in **Figure 5**. The domain spacing and relative root-mean-square composition variations σ are inferred from the long period and integrated scattering intensity, respectively,[55] and listed in **Table 3**. The domain spacing and relative σ are increased from PM6: Y6, PM6: Y6-1O to PM6: Y6-2O, which agrees well with the aggregation change from Y6, Y6-1O to Y6-2O. However, the domain spacing of PM6: Y6-2O blend is about 78 nm, which is probably too large for optimal OPV operation.[56-58] To investigate the surface morphology of the three blends, atomic force microscopy (AFM) was used to obtain the height and phase images of the three blends shown in **Figure S4** and **Figure S5**. The AFM results indicate that all three blends show smooth surfaces. Overall, these results are consistent with the general effects of alkoxy groups on morphology and explain the performance differences of the three molecules.[44]

To study the alkoxy substitution effect on charge mobility, the hole and electron mobilities ($\mu_h$ and $\mu_e$) were measured using the space-charge-limited-current (SCLC, **Figure S6**) method. As shown in **Table 2**, the hole mobilities of three blends are similar while the

electron mobilities differ a lot. PM6: Y6-1O blends exhibit a slightly higher $\mu_e$ of $7.8 \times 10^{-4}$ $cm^2$ $V^{-1}$ $s^{-1}$ than the PM6: Y6 ones ($5.18\times10^{-4}$ $cm^2$ $V^{-1}$ $s^{-1}$), which contributes to the slightly higher FF of OSCs based on Y6-1O. PM6: Y6-2O blends show the worst $\mu_e$ of $8.0 \times 10^{-5}$ $cm^2$ $V^{-1}$ $s^{-1}$, which might be due to the poor solubility and film quality (as a highly crystalline semiconductor could also have low mobility if the molecules form isolated crystalline domains with poor inter-domain connections). Overall, the asymmetric alkoxy and alkyl substitution can slightly improve $\mu_e$, thus improve the FF of the devices.

To better understand the difference of $J_{sc}$ and FF among Y6-2O, Y6-1O and Y6 based devices, the exciton dissociation and charge collection properties of the three OSCs were studied by measuring their photocurrent density ($J_{ph}$) as a function of effective voltage ($V_{eff}$). Herein, $J_{ph}$ is referred as $J_{ph} = J_L - J_D$, where $J_L$ and $J_D$ are the current densities under light and in the dark condition, while $V_{eff}$ is defined as $V_{eff} = V_0 - V_{app}$, where $V_0$ is the voltage when $J_{ph} = 0$ and $V_{app}$ is the applied external voltage.[59] As shown in **Figure 6a**, PM6: Y6-1O and PM6: Y6 based devices can reach their saturated $J_{ph}$ at a relative low $V_{eff}$ of 0.6 V while the $J_{ph}$ of PM6: Y6-2O based devices gets closed to saturated at much higher $V_{eff}$ of >2 V, which can be explained by the low electron mobility of PM6: Y6-2O blends. Here the $J_{ph}$ at the $V_{eff}$ of 3.0 V were chosen as saturated $J_{ph}$ ($J_{sat}$) and the charge dissociation probability *P(E,T)* can be obtained from $J_{ph}/J_{sat}$. Under short-circuit and maximal power output (MPP) conditions, the *P(E,T)* of PM6: Y6-1O and PM6: Y6 based devices are calculated to be similar as 97.4%/88.7% and 97.7%/87.6% (**Table S3**). But for PM6: Y6-2O based devices, the corresponding *P(E,T)* are determined to be much lower as 89.9%/66.2%, indicating a lower

exciton dissociation probability and weaker charge collection efficiency compared to those of Y6-1O and Y6 based devices.

Furthermore, we measured the *J-V* curves of the three OSCs under different light intensity (*P*) to figure out degrees of bimolecular recombination and trap-assisted recombination. Under different light intensity, the corresponding $J_{sc}$ and *P* would comply with the expression of $J_{sc} \propto P^{S}$.[60, 61] If S is closer to 1, the less bimolecular recombination will occur. In addition, under the open-circuit condition of different light intensity, the $V_{oc}$ and *P* follow the formula of $V_{oc} \propto n(KT/q)\ln(P)$, where *n*, *q*, *T*, and *K* are the ideality factor, the elementary charge, temperature (K) and Boltzmann constant, respectively. The smaller *n* value suggests reduced trap-assisted recombination.[62] **Figure 6b** shows the $J_{sc}$ versus *P* plots in a double logarithmic scale mode and **Figure 6c** depicts the $V_{oc}$ versus *P* plots where *P* is in natural logarithmic scale mode. The S values of the Y6-2O, Y6-1O and Y6 based devices are derived to be 0.973, 0.980, 0.972. The S values for the three devices are similar and close to 1, which indicates that bimolecular recombination is not determining factor in the device performances of the three OSCs. The *n* values extracted from the curves of **Figure 6c** are 1.29, 1.12, 1.10 for PM6: Y6-2O, PM6: Y6-1O and PM6: Y6 based devices, respectively, indicating PM6: Y6-2O based OSCs suffer from more severe trap-assisted recombination than the other two devices and thus leads to low $J_{sc}$ and FF.

We further employed the transient photocurrent (TPC) at a short-circuit condition to assess the charge extraction capability of Y6, Y6-1O and Y6-2O based devices. Through fitting the

curves in **Figure 6d** with exponential decay function, the photocurrent decay times are 0.350, 0.355 and 0.313 μs for PM6: Y6-2O, PM6: Y6-1O and PM6: Y6 based devices. The similar decay times suggest the similar charge extraction capability with similar bimolecular recombination.[63] Under the open-circuit condition, transient photovoltage (TPV) is used to evaluate the lifetimes of charge carriers, which imply the degree of recombination. Through fitting the curves in **Figure 6e** with exponential decay function, the carrier lifetimes of PM6: Y6-2O, PM6: Y6-1O and PM6: Y6 based devices are 0.392, 0.537 and 0.456 μs, respectively. The higher carrier lifetimes mean lower recombination.[64] Therefore, the PM6: Y6-1O based OSCs with the lowest recombination can achieve excellent EQE and FF while the PM6: Y6-2O based devices with the highest recombination have poor EQE and FF.

To further enhance the device performance based on Y6-1O, [6,6]-Phenyl C71 butyric acid methyl ester ($PC_{71}BM$, the structure and energy levels shown in **Figure S7** and **Figure 1c**) was added as the third component to make the ternary OSCs.[65] The structure of ternary devices and processing conditions are the same as the binary devices except that the weight ratio of PM6, Y6-1O and $PC_{71}BM$ is 1: 1.2: 0.2. Compared to the performance of the PM6: Y6-1O binary system, the PM6: Y6-1O: $PC_{71}BM$ based devices can obtain higher $J_{sc}$ of 24.9 mA $cm^{-2}$ and FF of 78.5%, which helps to achieve better performances of 17.6% (**Table 2**). As shown in **Figure 3b**, PM6: Y6-1O: $PC_{71}BM$ based OSCs exhibit higher EQE than that of PM6: Y6-1O based devices, which agrees well with the corresponding $J_{sc}$. The higher $J_{sc}$ and EQE can be explained by the PL quenching spectrum listed in **Figure 3d** that the PL quenching efficiency of the ternary system is much higher than that of the binary system

(99.1% versus 95.7%). Also, $PC_{71}BM$ can increase electron mobility (**Table 2**), reduce the degree of bimolecular and trap-assisted recombination (**Figure 6b and 6c**) and enhance the lifetimes of carriers (**Figure 6e,** 0.746 μs), which is beneficial for high FF. Moreover, the addition of $PC_{71}BM$ can help achieve better morphology as confirmed by GIWAXS and R-SoXS data. As shown in **Table 3**, the coherence length of the π-π stacking in (010) direction for PM6: Y6-1O: $PC_{71}BM$ blends is improved, compared to that of PM6: Y6-1O blends. The PM6: Y6-1O: $PC_{71}BM$ blends exhibit the multi-length scale morphology with a low-q peak at ~0.11 $nm^{-1}$ and a high-q peak at ~0.324 $nm^{-1}$, which indicates a different phase separation kinetics compared to the of PM6: Y6-1O blends. Therefore, PM6: Y6-1O: $PC_{71}BM$ based OSCs can achieve excellent performance of 17.6% with high $J_{sc}$ and FF.

## Conclusion

In conclusion, we designed and synthesized two novel NFAs named Y6-1O and Y6-2O by replacing the alkyl chain (s) on the β-position of the outer thiophene unit in Y6 with the alkoxy side chain (s). Although Y6-2O has the highest LUMO level due to one alkoxy chain on each side, its poor solubility in chloroform leads to poor morphology and low device performance. Due to the asymmetric alkoxy and alkyl substitution, Y6-1O obtains a higher LUMO level while keeping reasonably good solubility, which helps corresponding devices to achieve higher $V_{oc}$ of 0.89 V, $J_{sc}$ of 23.2 mA $cm^{-2}$ and FF of 78.3%. All these parameters combined lead to a high PCE of 16.1% in PM6: Y6-1O based devices but the poor performance of 6.6% in PM6: Y6-2O based devices. Further addition of $PC_{71}BM$ to the

binary blends leads to even higher $J_{sc}$ and FF and an excellent PCEs of 17.6%. This novel strategy of asymmetric alkyl and alkoxy substitution takes advantages of alkoxy groups and avoid solubility problem, which can be applied to other NFAs especially Y-series molecules to push the efficiencies to a higher level.

## Tables and Figures

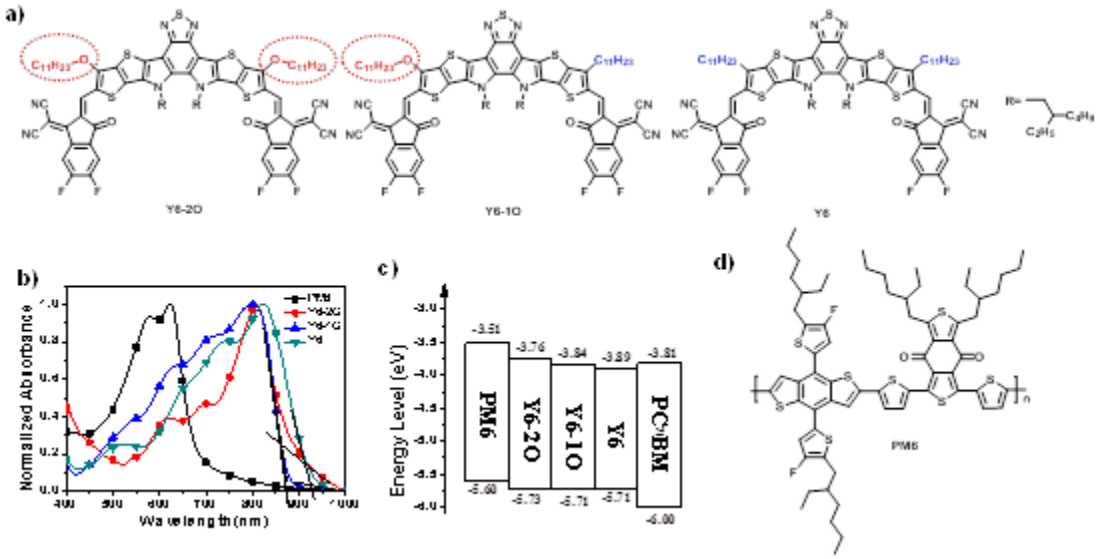


**Figure 1.** a) The chemical structures of Y6-2O, Y6-1O and Y6; b) Normalized absorption spectra of PM6, Y6-2O, Y6-1O and Y6 in neat films; c) The energy level plot of PM6, Y6-2O, Y6-1O, Y6 and $PC_{71}BM$; d) The chemical structure of PM6.

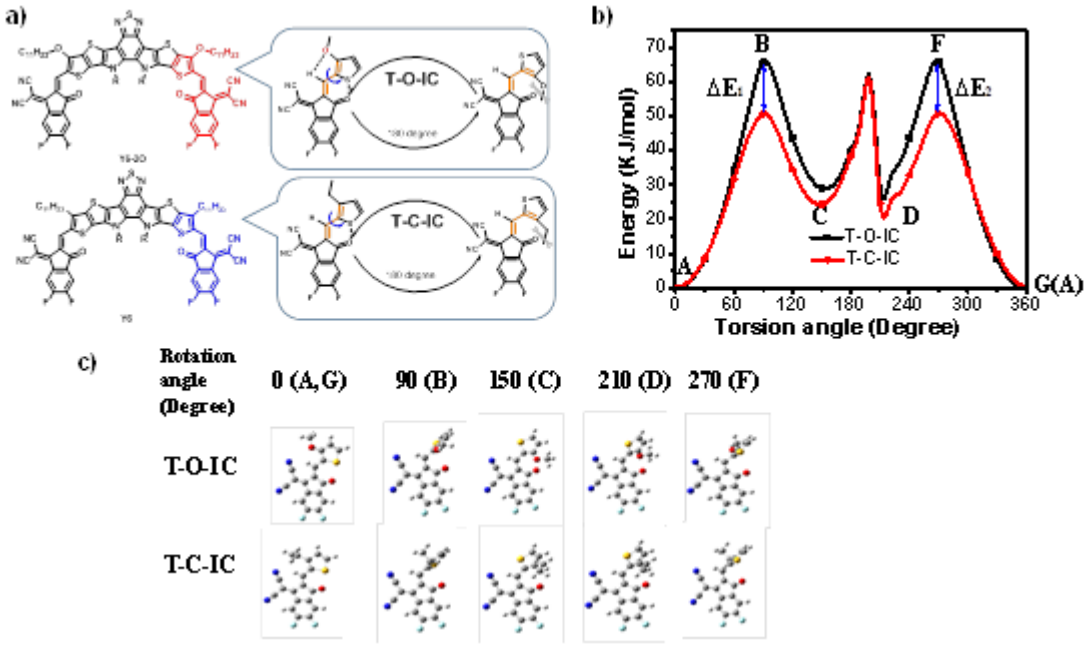


**Figure 2.** a) Diagram of torsion for T-O-IC and T-C-IC; b) Relaxed potential energy scan results of T-O-IC and T-C-IC (36 steps of size 10 degrees); c) Conformation of T-O-IC and T-C-IC in the key spots of the relaxed potential energy scan plot.

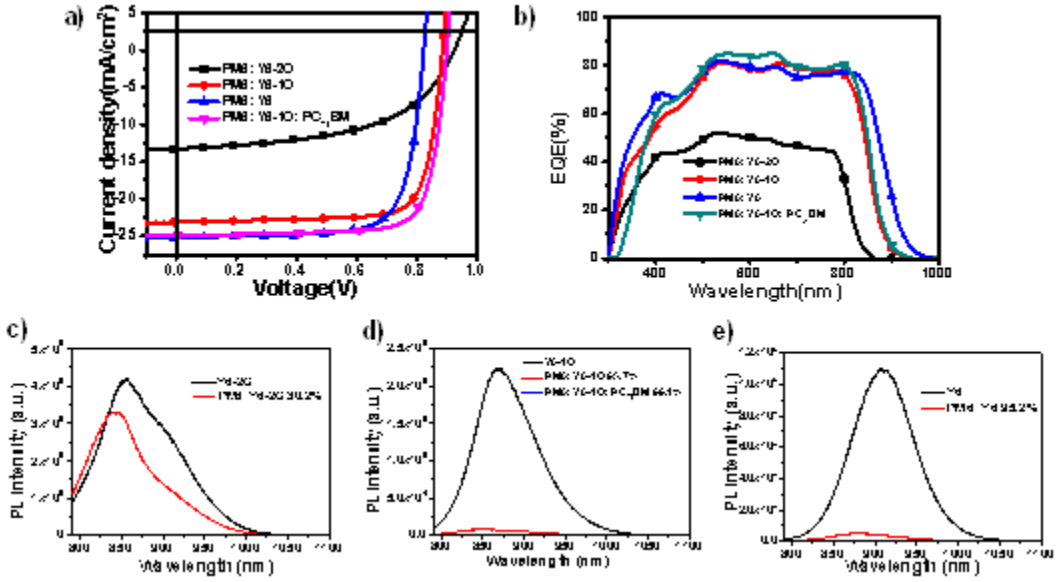


**Figure 3**. a) Current density-voltage (*J-V)* curves of OSCs based on PM6: Y6-2O, PM6: Y6-1O, PM6: Y6 and PM6: Y6-1O: $PC_{71}BM$; b) Corresponding EQE spectrum; c) Photoluminescence quenching spectrum of Y6-2O and PM6: Y6-2O films excited at 785 nm; d) Photoluminescence quenching spectrum of Y6-1O, PM6: Y6-1O and PM6: Y6-1O: $PC_{71}BM$ films excited at 785 nm; e) Photoluminescence quenching spectrum of Y6 and PM6: Y6 films excited at 785 nm.

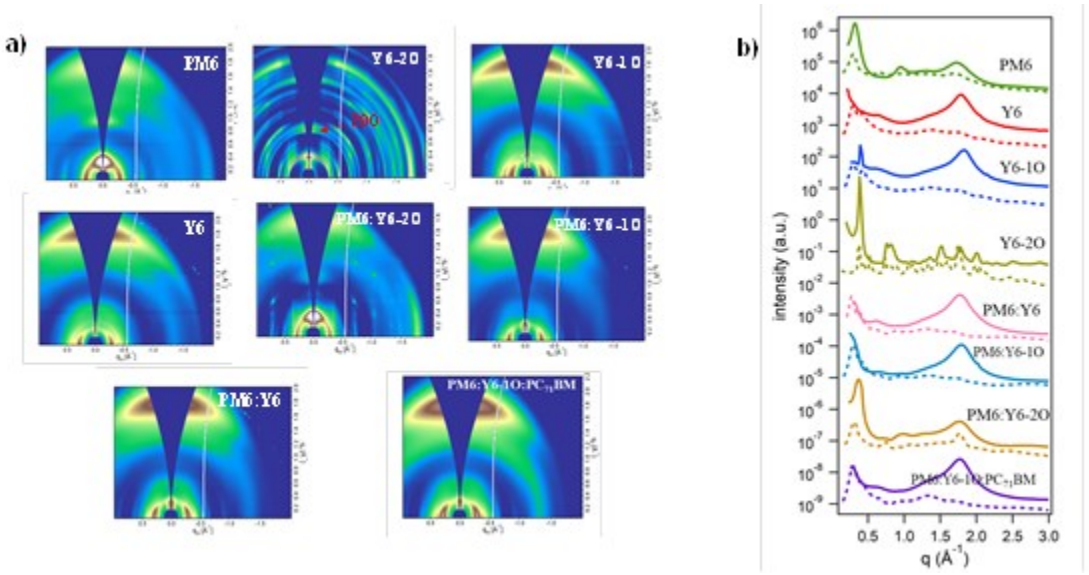


**Figure 4.** a) 2D-GIWAXS patterns: a neat PM6 film, a neat Y6-2O film, a neat Y6-1O film, a neat Y6 film, a PM6: Y6-2O blend film, a PM6: Y6-1O blend film, a PM6: Y6 blend film and a PM6: Y6-1O: $PC_{71}BM$ blend film; b) In-plane (dashed) and out-of-plane (solid) 10° sector averaged GIWAXS profiles of the corresponding 2D patterns.

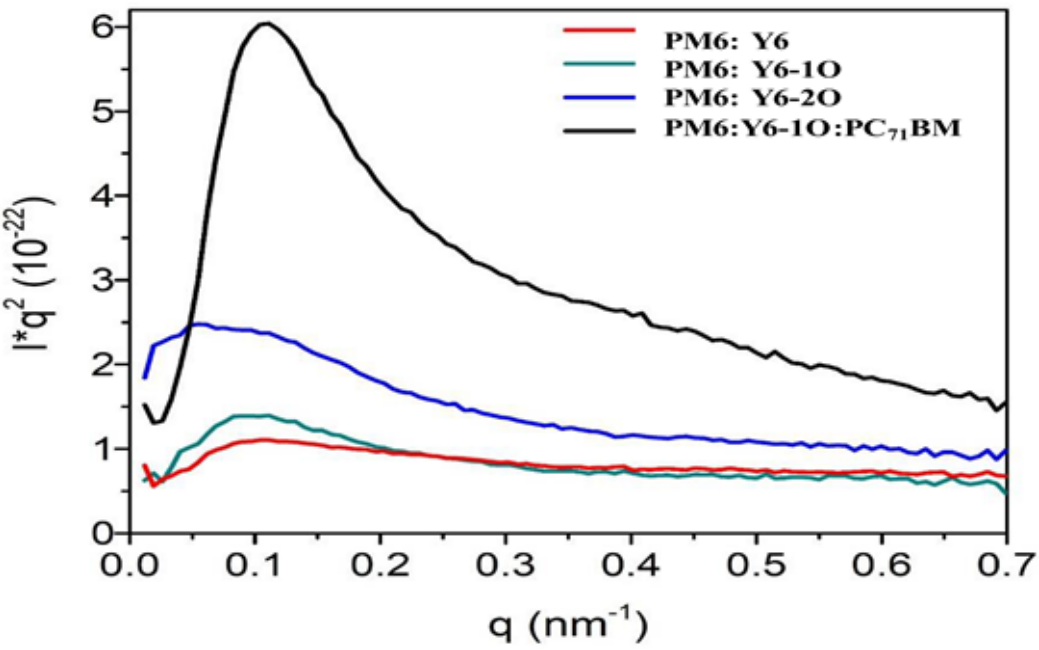


**Figure 5.** Film thickness and material contrast normalized, and Lorentz- and background corrected R-SoXS profiles of PM6: Y6-2O, PM6: Y6-1O, PM6: Y6 and PM6: Y6-1O: $PC_{71}BM$ based blend films.

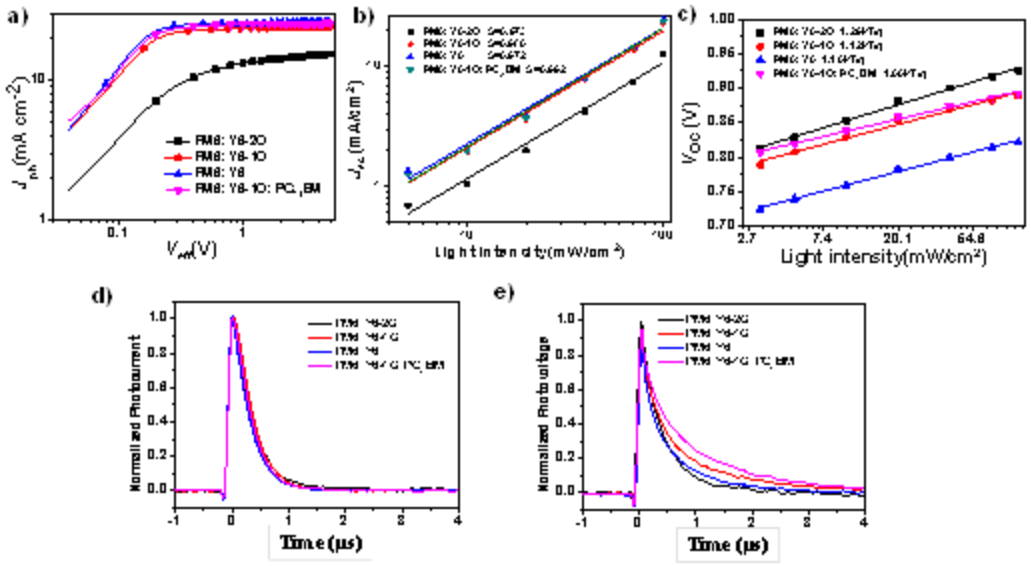


**Figure 6.** a) $J_{ph}$ versus $V_{eff}$ of the optimized devices; b) $J_{SC}$ versus light intensity; c) $V_{OC}$ versus light intensity; d) Transient photocurrent (TPC) measurements of Y6-2O, Y6-1O and Y6 based devices excited at 750 nm; e) transient photovoltage (TPV) measurements of Y6-2O, Y6-1O and Y6 based devices excited at 750 nm.

**Table 1.** The optical and electronic properties of Y6-2O, Y6-1O and Y6

| Acceptor | $\lambda_{max}$ [a] (nm) | $\lambda_{onset}$ [a] (nm) | $\lambda_{onset}$ [b] (nm) | $E_g$ [c] (eV) | HOMO [d] (eV) | LUMO [d] (eV) |
|---|---|---|---|---|---|---|
| **Y6-2O** | 701 | 741 | 858 | 1.45 | -5.73 | -3.76 |
| **Y6-1O** | 715 | 764 | 870 | 1.43 | -5.71 | -3.84 |
| **Y6** | 732 | 783 | 922 | 1.35 | -5.71 | -3.89 |

[a] In chloroform solution. [b] In a neat film. [c] Calculated from the empirical formula: $E_g = 1240/\lambda_{onset}$ [b]. [d] Using cyclic voltammetry (CV) method.

**Table 2.** The optimal photovoltaic parameters of Y6-2O, Y6-1O and Y6 based OCSs.

| Active layer | $V_{oc}$ (V) | $J_{sc}$ (mA cm$^{-2}$) [a] | FF (%) | PCE (%) [b] | $\mu_h$(cm$^2$ V$^{-1}$ s$^{-1}$) [c] | $\mu_e$(cm$^2$ V$^{-1}$ s$^{-1}$) [c] |
|---|---|---|---|---|---|---|
| **PM6: Y6-2O** | 0.92 | 13.3 (13.2) | 53.5 | 6.6 (5.6) | $8.4\times10^{-4}$ | $8.0\times10^{-5}$ |
| **PM6: Y6-1O** | 0.89 | 23.2 (23.0) | 78.3 | 16.1 (15.4) | $8.2\times10^{-4}$ | $7.8\times10^{-4}$ |
| **PM6: Y6** | 0.82 | 25.3 (24.9) | 75.5 | 15.7 (15.2) | $6.6\times10^{-4}$ | $5.2\times10^{-4}$ |
| **PM6: Y6-1O: $PC_{71}BM$** | 0.90 | 24.9 (24.4) | 78.5 | 17.6 (17.4) | $8.1\times10^{-4}$ | $1.3\times10^{-3}$ |

[a] The values in bracket are integrated $J_{sc}$ from EQE spectra. [b] The values in bracket are the average PCE of 20 devices. [c] Measured by space charge limited current (SCLC) method

**Table 3.** Morphological parameters obtained from R-SoXS and GIWAXS.

| Samples | **RSoXS** | | **(010) peak** | | | |
|---|---|---|---|---|---|---|
| | Domain spacing[a] (nm) | Relative σ[b] | location ($Å^{-1}$) | *d*-spacing[c] (Å) | FWHM (A^-1) | CL[d] (Å) |
| PM6 | - | - | 1.74 | 3.61 | 0.24 | 26 |
| Y6-2O | - | - | 1.76 | 3.57 | 0.053 | 119 |
| Y6-1O | - | - | 1.81 | 3.47 | 0.21 | 30 |
| Y6 | - | - | 1.79 | 3.51 | 0.21 | 30 |
| PM6: Y6-2O | 78 | 1 | 1.76 | 3.57 | 0.25 | 25 |
| PM6: Y6-1O | 63 | 0.78 | 1.79 | 3.51 | 0.22 | 29 |
| PM6: Y6 | 53 | 0.67 | 1.77 | 3.55 | 0.20 | 31 |
| PM6: Y6-1O: $PC_{71}BM$[e] | 59 | 0.71 | 1.79 | 3.51 | 0.17 | 37 |
| | 19 | | | | | |

[a] Obtained by the equation of $\zeta = 2\pi/q$, in which $q$ is the corresponding x-coordinate of maximum peak in scattering intensity [b] Extracted by integrating scattering profiles [c] Obtained by the equation of $d = 2\pi/q$, in which $q$ is the corresponding x-coordinate of diffraction peak. [d] Calculated using the equation: $CL = 2\pi K/w$, in which w is the full width at half maxima and K is a form factor. [e] Domain spacing is calculated by a low-q peak and a high-q peak of corresponding R-SoXS profiles.

## Experimental Section

### Materials, device fabrication and characterization

The detailed synthetic procedure of Y6-1O and Y6-2O, the source of electron donors PM6 and device fabrication and characterization details are provided in the Supporting Information.

### GIWAXS characterization

GIWAXS measurements were performed at beamline 7.3.3 at the Advanced Light Source, LBNL. Samples were prepared on Si substrates using identical blend solutions like those used in devices. The 10 keV X-ray beam was incident at a grazing angle of 0.11° - 0.15°, The scattered X-rays were detected using a Dectris Pilatus 2M photon-counting detector.

### R-SoXS characterization

R-SoXS transmission measurements were performed at beamline 11.0.1.2 at the Advanced Light Source, LBNL. Samples for R-SoXS measurement were prepared on a PSS modified Si substrate under the same conditions as those used for device fabrication, and then transferred by floating in water to a 1.5 mm × 1.5 mm, 100 nm thick $Si_3N_4$ membrane supported by a 5 mm × 5 mm, 200 μm thick Si frame (Norcada Inc.). 2D scattering patterns were collected on an in-vacuum S5 CCD camera (Princeton Instrument PI-MTE). The sample detector distance was calibrated from diffraction peaks of a triblock copolymer poly

(isoprene-b-styrene-b-2-vinyl pyridine), which has a known spacing of 391 Å. The beam size at the sample is approximately 100 μm by 200 μm.

## Supporting Information

All data needed to evaluate the conclusions in the paper are present in the paper and/or the Supporting Information. Additional data related to this paper may be requested from the authors.

## Acknowledgements

Y. Chen and F. Bai contributed equally to this work. H.Y. acknowledges the National Key Research and Development Program of China (No. 2019YFA0705900) funded by MOST, the Shen Zhen Technology and Innovation Commission (project number JCYJ20170413173814007, JCYJ20170818113905024), the Basic and Applied Basic Research Major Program of Guangdong Province (No. 2019B030302007), the Hong Kong Research Grants Council (Research Impact Fund R6021-18, project numbers 16305915, 16322416, 606012, and 16303917) and Hong Kong Innovation and Technology Commission for the support through projects ITC-CNERC14SC01 and ITS/471/18. Z.P., Y.Q. and H.A. were supported by an ONR grant N000141712204. GIWAXS and RSoXS data were acquired at beamlines 7.3.3 and 11.0.1.2, respectively, at the Advanced Light Source, LBNL, which is supported by the Director, Office of Science, Office of Basic Energy Sciences, of the U.S. Department of Energy under Contract No. DE-AC02-05CH11231. L.Z. and F.L. were financially supported by the grant from the National Natural Science Foundation of China

(Nos. 21734009, 11327902, 11574204, 11774224, and 21822505) and National Key Research and Development Program of China (2017YFA0207700).

## Conflicts of interest

The authors declare no competing interests.

## Reference

[1] F. Huang, Z. Bo, Y. Geng, X. Wang, L. Wang, Y. Ma, J. Hou, W. Hu, J. Pei, H. Dong, S. Wang, Z. Li, Z. Shuai, Y. Li, Y. Cao, *Acta Polymerica Sinica* **2019**, *50*, 988.

[2] P. Cheng, G. Li, X. Zhan, Y. Yang, *Nat. Photonics* **2018**, *12*, 131.

[3] A. Wadsworth, M. Moser, A. Marks, M. S. Little, N. Gasparini, C. J. Brabec, D. Baran, I. McCulloch, *Chem. Soc. Rev.* **2019**, *48*, 1596.

[4] C. Yan, S. Barlow, Z. Wang, H. Yan, A. K. Y. Jen, S. R. Marder, X. Zhan, *Nat. Rev. Mater.* **2018**, *3*, 18003.

[5] J. Hou, O. Inganäs, R. H. Friend, F. Gao, *Nat. Mater.* **2018**, *17*, 119.

[6] G. Zhang, J. Zhao, P. C. Y. Chow, K. Jiang, J. Zhang, Z. Zhu, J. Zhang, F. Huang, H. Yan, *Chem. Rev.* **2018**, *118*, 3447.

[7] X. Du, T. Heumueller, W. Gruber, A. Classen, T. Unruh, N. Li, C. J. Brabec, *Joule* **2019**, *3*, 215.

[8] D. Baran, R. S. Ashraf, D. A. Hanifi, M. Abdelsamie, N. Gasparini, J. A. Röhr, S. Holliday, A. Wadsworth, S. Lockett, M. Neophytou, C. J. M. Emmott, J. Nelson, C. J. Brabec, A. Amassian, A. Salleo, T. Kirchartz, J. R. Durrant, I. McCulloch, *Nat. Mater.* **2017**, *16*, 363.

[9] L. Meng, Y. Zhang, X. Wan, C. Li, X. Zhang, Y. Wang, X. Ke, Z. Xiao, L. Ding, R. Xia, H.-L. Yip, Y. Cao, Y. Chen, *Science* **2018**, *361*, 1094.

[10] Y. Cui, H. Yao, J. Zhang, T. Zhang, Y. Wang, L. Hong, K. Xian, B. Xu, S. Zhang, J. Peng, Z. Wei, F. Gao, J. Hou, *Nat. Commun.* **2019**, *10*, 2515.

[11] Z. Zhou, W. Liu, G. Zhou, M. Zhang, D. Qian, J. Zhang, S. Chen, S. Xu, C. Yang, F. Gao, H. Zhu, F. Liu, X. Zhu, *Adv. Mater.* **2020**, *32*, 1906324.

[12] T. Yan, W. Song, J. Huang, R. Peng, L. Huang, Z. Ge, *Adv. Mater.* **2019**, *31*, 1902210.

[13] X. Xu, K. Feng, Z. Bi, W. Ma, G. Zhang, Q. Peng, *Adv. Mater.* **2019**, *31*, 1901872.

[14] H. Sun, T. Liu, J. Yu, T.-K. Lau, G. Zhang, Y. Zhang, M. Su, Y. Tang, R. Ma, B. Liu, J. Liang, K. Feng, X. Lu, X. Guo, F. Gao, H. Yan, *Energy Environ. Sci.* **2019**, *12*, 3328.

[15] C. Sun, S. Qin, R. Wang, S. Chen, F. Pan, B. Qiu, Z. Shang, L. Meng, C. Zhang, M. Xiao, C. Yang, Y. Li, *J. Am. Chem. Soc.* **2020**, *142*, 1465.

[16] J. Song, C. Li, L. Zhu, J. Guo, J. Xu, X. Zhang, K. Weng, K. Zhang, J. Min, X. Hao, Y. Zhang, F. Liu, Y. Sun, *Adv. Mater.* **2019**, *31*, 1905645.

[17] Y. Lin, B. Adilbekova, Y. Firdaus, E. Yengel, H. Faber, M. Sajjad, X. Zheng, E. Yarali, A. Seitkhan, O. M. Bakr, A. El-Labban, U. Schwingenschlögl, V. Tung, I. McCulloch, F. Laquai, T. D. Anthopoulos, *Adv. Mater.* **2019**, *31*, 1902965.

[18] S. Liu, J. Yuan, W. Deng, M. Luo, Y. Xie, Q. Liang, Y. Zou, Z. He, H. Wu, Y. Cao, *Nat. Photonics* **2020**, *14*, 300.

[19] L. Liu, Y. Kan, K. Gao, J. Wang, M. Zhao, H. Chen, C. Zhao, T. Jiu, A.-K. Y. Jen, Y. Li, *Adv. Mater.* **2020**, *32*, 1907604.

[20] J. Yuan, Y. Zhang, L. Zhou, G. Zhang, H.-L. Yip, T.-K. Lau, X. Lu, C. Zhu, H. Peng, P. A. Johnson, M. Leclerc, Y. Cao, J. Ulanski, Y. Li, Y. Zou, *Joule* **2019**, *3*, 1140.

[21] J. Yuan, T. Huang, P. Cheng, Y. Zou, H. Zhang, J. L. Yang, S.-Y. Chang, Z. Zhang, W. Huang, R. Wang, D. Meng, F. Gao, Y. Yang, *Nat. Commun.* **2019**, *10*, 570.

[22] L. Perdigón-Toro, H. Zhang, A. Markina, J. Yuan, S. M. Hosseini, C. M. Wolff, G. Zuo, M. Stolterfoht, Y. Zou, F. Gao, D. Andrienko, S. Shoaee, D. Neher, *Adv. Mater.* **2020**, *32*, 1906763.

[23] K. Jiang, Q. Wei, J. Y. L. Lai, Z. Peng, H. K. Kim, J. Yuan, L. Ye, H. Ade, Y. Zou, H. Yan, *Joule* **2019**, *3*, 3020.

[24] L. Hong, H. Yao, Z. Wu, Y. Cui, T. Zhang, Y. Xu, R. Yu, Q. Liao, B. Gao, K. Xian, H. Y. Woo, Z. Ge, J. Hou, *Adv. Mater.* **2019**, *31*, 1903441.

[25] Y. Cui, H. Yao, L. Hong, T. Zhang, Y. Tang, B. Lin, K. Xian, B. Gao, C. An, P. Bi, W. Ma, J. Hou, *Natl. Sci. Rev.* **2019**.

[26] Y. Li, L. Zhong, B. Gautam, H.-J. Bin, J.-D. Lin, F.-P. Wu, Z. Zhang, Z.-Q. Jiang, Z.-G. Zhang, K. Gundogdu, Y. Li, L.-S. Liao, *Energy Environ. Sci.* **2017**, *10*, 1610.

[27] Y. Li, J.-D. Lin, X. Che, Y. Qu, F. Liu, L.-S. Liao, S. R. Forrest, *J. Am. Chem. Soc.* **2017**, *139*, 17114.

[28] Y. Liu, M. Li, X. Zhou, Q.-Q. Jia, S. Feng, P. Jiang, X. Xu, W. Ma, H.-B. Li, Z. Bo, *ACS Energy Lett.* **2018**, *3*, 1832.

[29] Y. Xie, W. Huang, Q. Liang, J. Zhu, Z. Cong, F. Lin, S. Yi, G. Luo, T. Yang, S. Liu, Z. He, Y. Liang, X. Zhan, C. Gao, H. Wu, Y. Cao, *ACS Energy Lett.* **2019**, *4*, 8.

[30] C. Sun, F. Pan, H. Bin, J. Zhang, L. Xue, B. Qiu, Z. Wei, Z.-G. Zhang, Y. Li, *Nat. Commun.* **2018**, *9*, 743.

[31] J. Wu, Y. Meng, X. Guo, L. Zhu, F. Liu, M. Zhang, *J. Mater. Chem. A* **2019**, *7*, 16190.

[32] Q. Liao, K. Yang, J. Chen, C. W. Koh, Y. Tang, M. Su, Y. Wang, Y. Yang, X. Feng, Z. He, H. Y. Woo, X. Guo, *ACS Appl. Mater. Interfaces* **2019**, *11*, 31119.

[33] X. Li, H. Huang, I. Angunawela, J. Zhou, J. Du, A. Liebman-Pelaez, C. Zhu, Z. Zhang, L. Meng, Z. Xie, H. Ade, Y. Li, *Adv. Funct. Mater.* **2020**, *30*, 1906855.

[34] J. Zhu, Y. Xiao, J. Wang, K. Liu, H. Jiang, Y. Lin, X. Lu, X. Zhan, *Chem. Mater.* **2018**, *30*, 4150.

[35] S. Li, L. Ye, W. Zhao, S. Zhang, H. Ade, J. Hou, *Adv. Energy Mater.* **2017**, *7*, 1700183.

[36] X. Guo, J. Quinn, Z. Chen, H. Usta, Y. Zheng, Y. Xia, J. W. Hennek, R. P. Ortiz, T. J. Marks, A. Facchetti, *J. Am. Chem. Soc.* **2013**, *135*, 1986.

[37] S. Shi, Q. Liao, Y. Tang, H. Guo, X. Zhou, Y. Wang, T. Yang, Y. Liang, X. Cheng, F. Liu, X. Guo, *Adv. Mater.* **2016**, *28*, 9969.

[38] H. Huang, Q. Guo, S. Feng, C. e. Zhang, Z. Bi, W. Xue, J. Yang, J. Song, C. Li, X. Xu, Z. Tang, W. Ma, Z. Bo, *Nat. Commun.* **2019**, *10*, 3038.

[39] Y. Liu, Z. Zhang, S. Feng, M. Li, L. Wu, R. Hou, X. Xu, X. Chen, Z. Bo, *J. Am. Chem. Soc.* **2017**, *139*, 3356.

[40] H. Yao, Y. Chen, Y. Qin, R. Yu, Y. Cui, B. Yang, S. Li, K. Zhang, J. Hou, *Adv. Mater.* **2016**, *28*, 8283.

[41] H. Yao, Y. Cui, R. Yu, B. Gao, H. Zhang, J. Hou, *Angew. Chem. Int. Ed.* **2017**, *56*, 3045.

[42] Y. Cui, C. Yang, H. Yao, J. Zhu, Y. Wang, G. Jia, F. Gao, J. Hou, *Adv. Mater.* **2017**, *29*, 1703080.

[43] S. Feng, C. e. Zhang, Y. Liu, Z. Bi, Z. Zhang, X. Xu, W. Ma, Z. Bo, *Adv. Mater.* **2017**, *29*, 1703527.

[44] Y. Liu, M. Li, J. Yang, W. Xue, S. Feng, J. Song, Z. Tang, W. Ma, Z. Bo, *Adv. Energy Mater.* **2019**, *9*, 1901280.

[45] H.-H. Gao, Y. Sun, Y. Cai, X. Wan, L. Meng, X. Ke, S. Li, Y. Zhang, R. Xia, N. Zheng, Z. Xie, C. Li, M. Zhang, H.-L. Yip, Y. Cao, Y. Chen, *Adv. Energy Mater.* **2019**, *9*, 1901024.

[46] S. Ming, C. e. Zhang, P. Jiang, Q. Jiang, Z. Ma, J. Song, Z. Bo, *ACS Appl. Mater. Interfaces* **2019**, *11*, 19444.

[47] M. Li, Y. Zhou, J. Zhang, J. Song, Z. Bo, *J. Mater. Chem. A* **2019**, *7*, 8889.

[48] C. Li, H. Fu, T. Xia, Y. Sun, *Adv. Energy Mater.* **2019**, *9*, 1900999.

[49] T. Liu, Z. Luo, Q. Fan, G. Zhang, L. Zhang, W. Gao, X. Guo, W. Ma, M. Zhang, C. Yang, Y. Li, H. Yan, *Energy Environ. Sci.* **2018**, *11*, 3275.

[50] S. Zhang, Y. Qin, J. Zhu, J. Hou, *Adv. Mater.* **2018**, *30*, 1800868.

[51] M. Zhang, X. Guo, W. Ma, H. Ade, J. Hou, *Adv. Mater.* **2015**, *27*, 4655.

[52] A. Hexemer, W. Bras, J. Glossinger, E. Schaible, E. Gann, R. Kirian, A. MacDowell, M. Church, B. Rude, H. Padmore, *J. Phys. Con. Ser.* **2010**, *247*, 012007.

[53] P. Müller-Buschbaum, *Adv. Mater.* **2014**, *26*, 7692.

[54] E. Gann, A. T. Young, B. A. Collins, H. Yan, J. Nasiatka, H. A. Padmore, H. Ade, A. Hexemer, C. Wang, *Rev. Sci. Instrum.* **2012**, *83*, 045110.

[55] L. Ye, H. Hu, M. Ghasemi, T. Wang, B. A. Collins, J.-H. Kim, K. Jiang, J. H. Carpenter, H. Li, Z. Li, T. McAfee, J. Zhao, X. Chen, J. L. Y. Lai, T. Ma, J.-L. Bredas, H. Yan, H. Ade, *Nat. Mater.* **2018**, *17*, 253.

[56] Y. Zhu, A. Gadisa, Z. Peng, M. Ghasemi, L. Ye, Z. Xu, S. Zhao, H. Ade, *Adv. Energy Mater.* **2019**, *9*, 1900376.

[57] J. Zhang, Y. Li, H. Hu, G. Zhang, H. Ade, H. Yan, *Chem. Mater.* **2019**, *31*, 6672.

[58] J. Zhang, Y. Li, Z. Peng, F. Bai, L.-K. Ma, H. Ade, Z. Li, H. Yan, *Mater. Chem. Front.* **2020**, *4*, 1729.

[59] N. Gasparini, M. Salvador, S. Strohm, T. Heumueller, I. Levchuk, A. Wadsworth, J. H. Bannock, J. C. de Mello, H.-J. Egelhaaf, D. Baran, I. McCulloch, C. J. Brabec, *Adv. Energy Mater.* **2017**, *7*, 1700770.

[60] S. R. Cowan, A. Roy, A. J. Heeger, *Phys. Rev. B* **2010**, *82*, 245207.

[61] L. J. A. Koster, V. D. Mihailetchi, H. Xie, P. W. M. Blom, *Appl. Phys. Lett.* **2005**, *87*, 203502.

[62] W. L. Leong, S. R. Cowan, A. J. Heeger, *Adv. Energy Mater.* **2011**, *1*, 517.

[63] J. Wang, Z. Zheng, D. Zhang, J. Zhang, J. Zhou, J. Liu, S. Xie, Y. Zhao, Y. Zhang, Z. Wei, J. Hou, Z. Tang, H. Zhou, *Adv. Mater.* **2019**, *31*, 1806921.

[64] F. Pan, C. Sun, Y. Li, D. Tang, Y. Zou, X. Li, S. Bai, X. Wei, M. Lv, X. Chen, Y. Li, *Energy Environ. Sci.* **2019**, *12*, 3400.

[65] H. Lu, J. Zhang, J. Chen, Q. Liu, X. Gong, S. Feng, X. Xu, W. Ma, Z. Bo, *Adv. Mater.* **2016**, *28*, 9559.

TOC

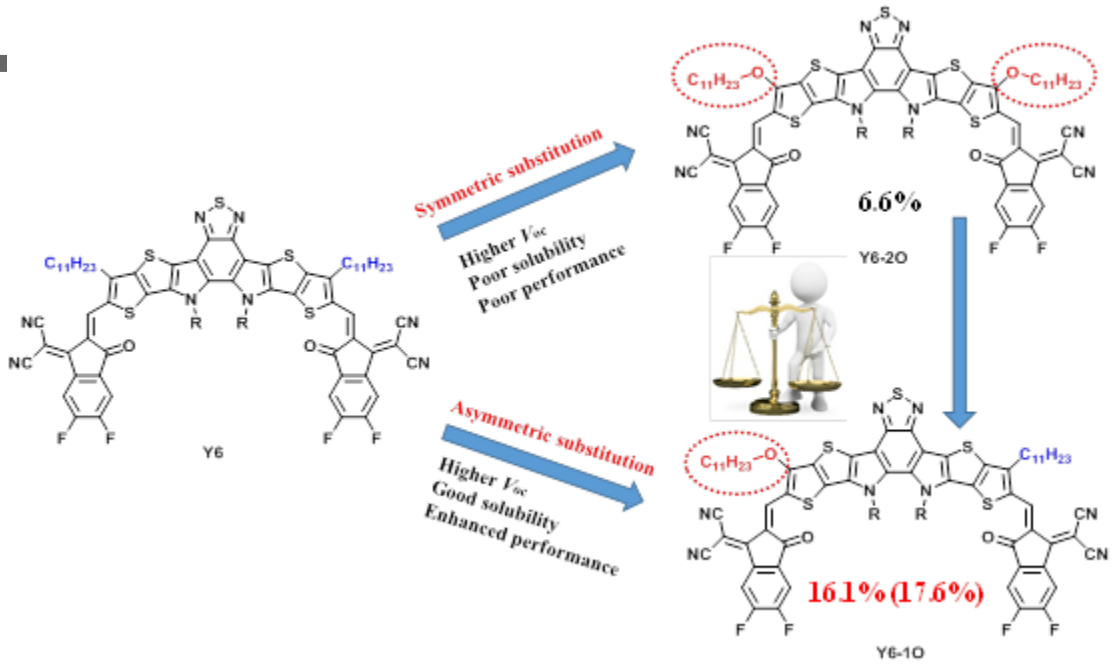


We adopted a novel asymmetric alkoxy and alkyl substitution on the well-known non-fullerene acceptor namely Y6 to get a new molecule named Y6-1O, and systematically compare its photoelectric properties and photovoltaic performance with the two symmetric molecules (Y6 and Y6-2O), which proves our design strategy is promising and effective.